$ReBaCo_{2-x}Mn_xO_{5+\delta}$ (Re: rare earth element) layered perovskites for application as cathodes in Solid Oxide Fuel Cells

Anna Olszewska[1,2],and *Konrad* Świerczek[1,2*]

[1]AGH University of Science and Technology, Faculty of Energy and Fuels, al. A. Mickiewicza 30, 30-059 Krakow, Poland
[2]AGH Centre of Energy, AGH University of Science and Technology, ul. Czarnowiejska 36, 30-054 Krakow, Poland

Abstract. Decrease of the operation temperature is considered as one of the most important targets in development of Solid Oxide Fuel Cells (SOFC), as it leads to considerable extension of their long-term operation and makes construction and utilization of the SOFC generators cost-effective. Relatively high value of the activation energy of the oxygen reduction reaction (ORR) occurring at the cathode, and consequently, large cathodic polarization resistance at lower temperatures is a major obstacle hindering usage of SOFCs at decreased temperatures. In this work possibility of application of manganese-doped cobalt-based cation-ordered perovskites as candidate cathode materials in the intermediate temperature (IT, ca. 600-800 °C) range is discussed. The considered oxide materials, depending on chemical composition, i.e. choice of Re element and Mn-doping level exhibit high values of mixed ionic-electronic conductivity, as well as good catalytic activity toward the oxygen reduction and moderate thermal expansion. Cathode layers manufactured on a basis of selected $ReBaCo_{2-x}Mn_xO_{5+\delta}$ oxides show low polarisation resistance.

1 Introduction

A major challenge facing today our planet is the observed climate change, which while not unambiguously, is considered to be interrelated with the anthropogenic emission of the greenhouse gases, such as carbon dioxide [1, 2]. This issue can be largely mitigated by development and implementation of the so-called clean energy sources, among which very promising ones are fuel cells [3–5]. Those devices are able to convert chemical energy of the fuels (such as hydrogen, syngas, but also hydrocarbons) and an oxidizer directly into electrical energy and heat, without need for the direct combustion, which is an intermediate step, indispensable in conventional thermomechanical methods of the electrical energy generation. As a result, fuel cells exhibit high conversion efficiency, especially in hybrid solutions, in which the waste heat is utilized. Their other advantages include short start-up time, zero emission if fuelled with hydrogen, easiness of modular scale-up and low failure

* Corresponding author: xi@agh.edu.pl

rates, due to a lack of moving, mechanical elements [6–8]. So far, numerous cell types, differing in a type of the applied electrolyte, have been designed. Among them, one of the most promising ones are Solid Oxide Fuel Cells (SOFC), showing wide fuel flexibility, exhibiting high energy conversion efficiency, and consequently, suitable for the broadest range of applications. Unfortunately, their very high operating temperature (typically, in 800-1000 °C range) may lead to a fast degradation, and therefore, current development of the SOFC technology is focused on new compounds (especially, anode and cathode materials, solid electrolytes), which are able to work effectively at the intermediate temperatures (ca. 600-800 °C). However, the target goal is to achieve good performance at even lower temperature range (ca. 400-600 °C) [9–13]. Presently, this seems to be the hardest in the case of cathode materials, due to high values of the activation energy of ORR, with associated substantial slowdown of ionic transport processes at decreased temperatures [12]. The overall effect is observed in a form of a high total polarisation resistance of the cathode, exceeding the commonly considered limit of 0.15 Ω cm^2.

In this work we discuss selected issues concerning design of new cathode materials from $ReBaCo_{2-x}Mn_xO_{5+\delta}$ (Re: rare earth element) system, having layered perovskite-type structure, which are suitable for manufacturing SOFC cathodes operating at lowered temperatures.

2 Decrease of the operation temperature as a crucial goal in development of SOFCs

As can be seen in Fig. 1, a typical Solid Oxide Fuel Cell is built with three basic elements: a cathode (where oxygen reduction occurs), an anode (where fuel oxidation occurs) and a dense and thin solid electrolyte, which is located between them and allows only for the ions (typically, oxygen anions) to be transferred from the cathode to the anode. Obviously, in SOFC stacks, design of interconnects and gas supply/removal systems is of a great importance.

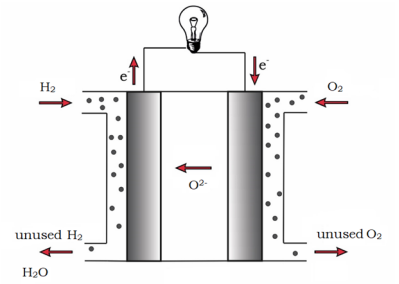

Oxygen reduction - cathodic reaction:
$½O_2 + 2e^- = O^{2-}$

Fuel (hydrogen) oxidation - anodic reaction:
$H_2 + O^{2-} = H_2O + 2e^-$
$CO + O^{2-} = CO_2 + 2e^-$
$CH_4 + 4O^{2-} = CO_2 + 2H_2O + 8e^-$

Fig. 1 Schematics of construction and operation of Solid Oxide Fuel Cell.

During last several decades, so-called YSZ (yttria stabilized zirconia, typically 8YSZ i.e. $Zr_{0.84}Y_{0.16}O_{1.92}$) has been the most commonly used electrolyte in SOFC technology, mostly due to its exceptional thermal stability and very good mechanical properties combined with rational price and acceptable, pure ionic conductivity. However, efficient operation of YSZ requires high temperatures, greatly exceeding 800 °C, unless very thin electrolyte layers are utilized [14]. Since lowering of the working temperature of SOFCs brings significant technical and economic benefits, such as reduction of the start-up time, increase of reliability, reduction of heat losses and also possibility of usage of cheaper, steel-based interconnects, research on novel electrolyte materials, which are able to efficiently operate at lowered temperatures has been extensively carried out [15–18]. Among proposed new compounds, Gd-doped ceria (GDC, $Ce_{1-x}Gd_xO_{2-\delta}$) and lanthanum gallate-based perovskites (LSGM, $La_{1-x}Sr_xGa_{1-y}Mg_yO_{3-\delta}$) are of a special interest, because of their very high ionic conductivity. In the anode-supported design with largely decreased electrolyte thickness, as well as with

usage of the improved electrode materials having tailored chemical composition and/or composite structure, it was already possible to reduce operating temperature of SOFCs down to ca. 800 °C range, maintaining high efficiently [12]. Recently, new reports have been presented in leading scientific journals about viability of further decrease of the operating temperature below ca. 600-650 °C, to the low temperature (LT) range [19–22]. It is anticipated that in such LT-SOFC designs lifetime of the cells can extend beyond 10 years, wider choice of electrode materials (including nanostructured designs), interconnects and seals will be available for usage, as well as reduced production and exploitation costs and easier balance of such SOFC-based generators will be very advantageous. Another important reason stems from the predicted increase of efficiency, e.g. if SOFC is using CO as a fuel, the theoretical efficiency increases from ca. 60% at 900 °C to ca. 80% at 350 °C [23]. Obviously, LT-SOFCs require highly-conductive electrolytes and thin, near to the submicron thickness, electrolyte layers to reduce the ohmic losses. Moreover, new electrode materials, especially for the cathode, need to be developed in order to reduce the polarization resistance [24]. It is generally assumed that for such the application, state-of-the-art solutions are needed. For example, modification of the bulk properties of the compounds, e.g. Co-based perovskite oxides, via chemical doping is conducted with untypical elements like Nb or Ta [22]. Alternatively, a combined approach dedicated to optimization of the bulk (lattice structure, electronic structure, concentration of defect species, etc.) and surface/microstructure (catalytically-active surfaces, exsoluted metallic nanoparticles, spatially-oriented morphology, etc.) is applied and showed to be successful [21,24–28].

3 Perovskite-type cathode materials: selected issues regarding structure and transport properties

Considering numerous and strict requirements regarding transport, electrocatalytic and thermomechanical properties, which need to be fulfilled by the successful air electrode (cathode) material, simple perovskites (with $ABO_{3-\delta}$ formula, e.g. $La_{1-x}Sr_xCo_{1-y}Fe_yO_{3-\delta}$) and cation-ordered, layered perovskite-based oxides ($AA'B_2O_{5+\delta}$, e.g. $GdBaCo_{2-x}Fe_xO_{5+\delta}$) are undoubtedly among the best candidates, and in fact, are being the most studied ones [5,7,29,30]. In the considered materials the electronic structure of BO_6 octahedra governs the charge transport properties in the bulk, while deviation from the oxygen stoichiometry, realized through presence of the oxygen vacancies, lowers the coordination number of B-site cations and enables ionic conduction. At the same time, surface-exposed sites with lowered oxygen coordination are considered as being responsible for the electrocatalytic activity of the compounds toward the ORR [27,31].

Compositional flexibility is one among the most important features of the perovskite-type materials, as through an appropriate doping strategy at A-, B- and even O-sites, modification of the structural and transport properties can be done [32]. In the case of substitution in cation sublattices, A- and B-site cation-ordered compounds are known. Such an ordering can be a result of a significant difference between ionic radii and/or oxidation state of ions present and the respective sites. For the 1:1 ratio, i.e. $AA'B_2O_{5+\delta}$ or $A_2BB'O_{5+\delta}$, the arrangement of ions can be generally realized as one of three different types: the rock salt-like, columnar and layered [33]. Considering $ReBaM_2O_{5+\delta}$ (Re: rare earth element; M: transition metal) layered compounds, the present layered-type arrangement of smaller Re^{3+} and larger Ba^{2+} cations is mainly caused by a large difference of their ionic radii. The crystal structure of such materials consist of BO_6 octahedra, between which layers containing barium or Re element are located alternately (Fig. 2a) [33]. It should be also mentioned that layered A-site ordering is often found in combination with a presence of anion vacancies, which helps to stabilize such the structure. Their concentration can reach high values, even close to 1 per formula unit, and therefore the common notation is in fact $ReBaM_2O_{5+\delta}$ (not $ReBaM_2O_{6-\delta}$). Such high

concentration of the oxygen vacancies and a fact that they are located almost exclusively between Re layers where oxygen bonding strength is reduced, leads to formation of a fast ion-conducting planes, enhancing significantly ionic component of the conductivity [33]. Consequently, the compounds are of a great interest considering possible application as cathode materials in SOFCs. In both, simple $ABO_{3-\delta}$ and layered $AA'B_2O_{5+\delta}$ perovskites, transport of electronic charge carries occurs through double-exchange (Zener) mechanism. Essential for this process is interaction of the 3*d* orbitals originating from the transition metal with the 2*p* orbitals of the oxygen, which can be simply described as a "jump" of the electron occurring through the metal-oxygen-metal path (Fig. 2b). The effectiveness of the whole process depends not only on degree of structural deviation (from cubic symmetry) and filling of the 3*d* states, but even more, on the oxygen content, as appearance of the oxygen vacancies interrupts metal-oxygen-metal paths. Therefore, the considered Zener-type mechanism is the most effective when compounds are fully oxidized, distortions in their structure are limited and present in the structure 3*d* metals exhibit mixed oxidation state [34,35].

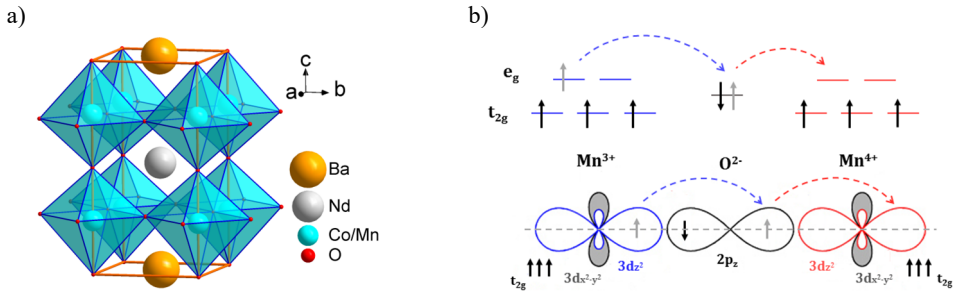

Fig. 2 a) Crystal structure of layered-type $ReBaM_2O_{5+\delta}$ oxide; **b)** scheme of a linear metal-oxygen-metal bond with possible Mn^{3+}-O-Mn^{4+} double exchange.

Simultaneously, oxygen concentration has the opposite effect on the ionic component of the conductivity, as relatively high oxygen nonstoichiometry causes increase of the effectiveness of ionic transport occurring through the vacancy-type mechanism. This process is particularly efficient in strongly oxygen-deficient layered-type perovskites, due to the mentioned appearance of the fast ion-conducting planes within the Re-related layers. To conclude, it can be stated that controlling of the oxygen content allows to obtain materials with desired/controlled ionic and electronic components of conductivity [34]. Among all double-perovskite oxides, cobaltites exhibits the highest values of total conductivity, with σ (predominantly electronic component) exceeding in many cases 1000 S cm^{-1} at room temperature. Such good transport properties results from highly-effective electron transfer occurring through the mentioned Zener mechanism [11,36]. It is generally known that substitution of cobalt with different 3*d* metals (such as iron or manganese) has generally negative impact on the total conductivity [35,37]. This behaviour can be explained taking the considered $ReBaCo_{2-x}Mn_xO_{5+\delta}$ group of materials as an example. Firstly, it must be emphasized that excellent electron transport in undoped cobaltites results from presence of Co^{4+}/Co^{3+} pairs and high mobility of the unpaired electron which can easily migrate between t_{2g} levels of Co^{3+} and Co^{4+}. This occurs with a high level of delocalization of the electrons, resulting in a metallic-like behaviour. Introduction of Mn into $ReBaCo_{2-x}Mn_xO_{5+\delta}$ structure causes charge transfer reaction to occur, as more stable manganese adopts +4 oxidation state and eliminates $Co^{4+/3+}$. Since average oxidation state of 3*d* metals is typically higher than 3 in considered materials, Mn^{4+}, Co^{3+} and Co^{2+} ions are present and further oxygen content loss leads to a decrease of concentration of Co^{3+} cations [18]. It is known that the polaron energy at the sites occupied by Mn^{4+} is lower than those occupied by Co^{4+}, and consequently, the effectiveness of the charge transfer in $ReBaCo_{2-x}Mn_xO_{5+\delta}$ for the Mn^{4+}/Mn^{3+} pair is

significantly smaller that for the Co^{4+}/Co^{3+} couple, but still it is larger than for the Mn^{4+}/Co^{3+} pair. Consequently, Mn-substitution into Co positions results in a decreased value of the electronic component of conductivity, whereas this negative influence is the most significant when Co:Mn ratio is equal to 1:1, as in this case the relative share of the worst conducting species (i.e. Mn^{4+}/Co^{3+}) is the highest. Moreover, introduction of Mn causes change of the conduction mechanism from a metallic-like, manifested by high values of the conductivity which decreases with increasing temperature, to the thermally activated behaviour, with the activation energy increasing with the Mn content [18,38]. Introduction of manganese into $ReBaCo_{2-x}Mn_xO_{5+\delta}$ oxides has another profound consequence, as the greater stability of its higher oxidation states (resulting from stronger Mn-O bonds) causes significantly lowered oxygen release at elevated temperatures in comparison with parent cobaltites. As a result, the associated formation of the oxygen vacancies affects less significantly electronic conductivity of Mn-doped materials [39,40]. Impact of Re cations on the total conductivity of the compounds is also visible. It is known that decreasing Re^{3+} size causes general decrease of σ, which directly results from lowered oxygen content leading to the mentioned disruption of the metal-oxygen-metal paths [35,36]. As presented for $ReBaCo_{2-x}Mn_xO_{5+\delta}$ group, in the case of other dopants, e.g. Fe, Ni, Cu, similar reasoning can be given regarding transport properties of the doped materials [13,41,42].

The mentioned compositional flexibility of perovskite-type oxides allows also to adjust parameters influencing electrocatalytic activity of the material toward the oxygen reduction reaction. As it was mentioned, sites with lowered oxygen coordination (e.g. BO_5, Fig. 3a) are present at the surface of the perovskite oxide. Such sites are particularly important for the ORR, since during the first step of the reaction oxygen molecules are adsorbed at the active sites (available at the surface of the cathode material). In this case, the crucial parameter is related to the filling of (surface) e_g states (Fig. 3b). Depending on the available electrons, oxygen molecules may form bonds with the surface [27,43].

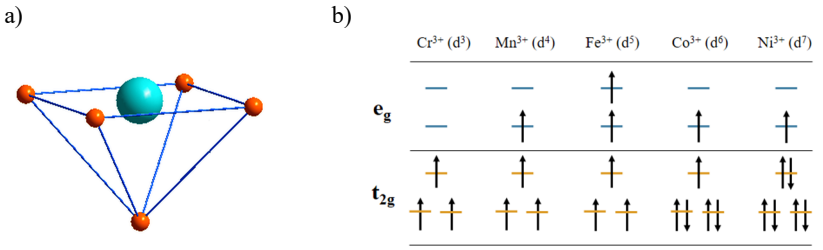

Fig. 3 a) Surface-exposed BO_5 pyramid with enhanced catalytic activity; **b)** filling of the e_g states in 3*d* metals (central atom in perovskite structure) for BO_5 configuration. Based on [27].

As shown experimentally, filling of the e_g states governs ORR activity in electrochemical aqueous oxygen reduction reaction, with the highest catalytic activity for the filling of e_g states close to 1 [27]. Similar behaviour may be expected at high temperatures (working cathode material in SOFCs). As can be seen in Fig. 3b, among basic 3*d* metals, the optimal filling of e_g states (≈ 1) is present for Co^{3+}, Mn^{3+} and Ni^{3+}.

Currently, cobalt-based oxides are undoubtedly considered as the most promising cathode materials among all perovskite-type compounds, due to their high electrocatalytic activity toward ORR and mixed ionic-electronic conductivity with the enhanced ionic component associated with high concentration of the oxygen vacancies, which all together lead to improved electrochemical performance in the IT range [13,15,44]. However, their practical application in SOFC technology is somewhat limited, due to the high thermal expansion coefficient (TEC), incompatible with the ones observed for the commonly used electrolyte materials. The mismatch in thermal expansion between components of the cell can result in

additional thermal stresses during the SOFC generator heating up and cooling down operations. Generally, the high TECs of cobalt-based oxides are mainly related to both, the oxygen loss and the associated reduction of smaller Co^{4+} (0.53 Å in the 6-fold coordination) to larger Co^{3+} (0.545 Å), as well as to the possible spin transitions of Co^{3+} [45–49]. As shown in the literature, this problem can be alleviated by substitution of Co with other 3*d* metals, such as copper, iron, but also, the discussed in this paper manganese [3,35,39,45]. While such the strategy is suitable to obtain efficient $ReBaCo_{2-x}M_xO_{5+\delta}$ cathodes operating at the intermediate temperatures, it is unfortunately insufficient if operation at the LT range is considered.

In order to obtain low values of the cathodic polarization resistance at temperatures below 600-650 °C, less typical doping approach of cobalt-based perovskites is conducted, with selected 4*d* and 5*d* elements (such as Nb, Mo, Ta and W) being involved. Those dopants give a unique combination of a relatively large ionic radius (stabilizing perovskite structure by adjustment of the so-called tolerance factor *t*), high charge state (affecting electronic structure, e_g filling and the oxygen content, and therefore, mixed ionic-electronic transport properties and catalytic activity), as well as electronegativity (influencing metal-oxygen bonds strength, which also modifies catalytic activity). As shown in the literature such the strategy combined with microstructural modification (i.e. nanoscale leading to increased specific surface area) allows to design materials with high Co content, working effectively even below 500 °C [22].

4 Overview of $ReBaCo_{2-x}Mn_xO_{5+\delta}$ as candidate cathode materials

$ReBaCo_{2-x}Mn_xO_{5+\delta}$ phase diagram has been studied relatively well with reported data on synthesis conditions of single-phase materials for different Co:Mn ratio and various Re^{3+} introduced (Fig. 4) [18,35,39,40]. Considered oxides were also evaluated in terms of their important physicochemical properties, such as crystal structure, oxygen content, thermal expansion and electrical conductivity. Moreover, possibility of their application as candidate cathode materials (chemical stability toward typical solid electrolytes; cathodic polarization resistance in a wide temperature range) has been evaluated.

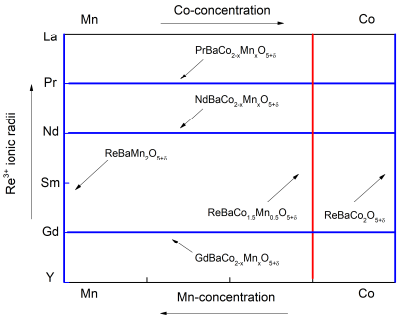

Fig. 4 Known phase diagram (blue and red lines) of cation-ordered $ReBaCo_{2-x}Mn_xO_{5+\delta}$ system.

Presence of the layered arrangement (or lack of it) in those materials depends on synthesis conditions (such as atmosphere and sintering temperature), as well as on the chemical composition (Re^{3+} radii and Mn:Co ratio) [18,35,39,40,45]. It is known that both, large Re^{3+} cations and high Mn concentration promote disordering of Re-Ba cations, with formation of cubic-like simple perovskite. On the contrary, Co-rich materials with introduced smaller Re^{3+} possess layered arrangement of Re-Ba (*P*4/*mmm* aristotype or related symmetry). To facilitate formation of the layered structure, the initial synthesis can be conducted in low pO_2 atmosphere (e.g. Ar), with final step related to the oxidation (e.g. in air) of the initially formed

$ReBaCo_{2-x}Mn_xO_{5+\delta}$. This approach was found to be effective especially for Mn-rich samples [35, 50]. Interested reader can find description of the structural properties of $ReBaCoMnO_{5+\delta}$ in [50] and $ReBaCo_{1.5}Mn_{0.5}O_{5+\delta}$ in [35]. Of importance, regardless of the adopted crystal structure, significant decrease of the thermal expansion coefficient with Mn incorporation in $ReBaCo_{2-x}Mn_xO_{5+\delta}$ was observed, with relationship being monotonically, but non-linearly dependent on the increasing Mn content. In Tab. 1 exemplary TEC values for basic undoped cobaltites, as well as for oxides substituted with different Mn ratio are presented. The observed decrease of TEC results from the reduced oxygen content change at elevated temperatures for Mn-doped materials (stronger Mn-O bonds) and vanishing of the spin-related thermal expansion (decreased amount of Co). Interestingly, the positive impact of the Mn presence on the thermal expansion diminishes if smaller Re^{3+} cations (such as Gd^{3+}) are introduced [35].

Tab. 1 Values of thermal expansion coefficient ($\cdot 10^{-6}$ K^{-1}) calculated in 300-800 °C (300-900 °C for Gd-containing oxides) range for selected $ReBaCo_{2-x}Mn_xO_{5+\delta}$ oxides.

Re^{3+}	$ReBaCo_2O_{5+\delta}$	$ReBaCo_{1.5}Mn_{0.5}O_{5+\delta}$	$ReBaCoMnO_{5+\delta}$	$ReBaCo_{0.5}Mn_{1.5}O_{5+\delta}$
Pr	26.6 [40]	21.0 [40]	16.6 [40]	-
Nd	24.8 [39]	21.0 [39]	18.4 [39]	13.9 [39]
Sm	23.1 [35]	20.5 [35]	19.4 this work	-
Gd	20.7 [35]	19.5 [35]	18.8 this work	-

The mentioned stronger Mn-O bonds result also in the increased oxygen content in Mn-doped samples at room temperature. For example, in Nd-containing materials the respective values increase from 5.7 for $NdBaCo_2O_{5+\delta}$ to 5.83 for $NdBaCo_{1.5}Mn_{0.5}O_{5+\delta}$ and to 5.94 for $NdBaCoMnO_{5+\delta}$ [35]. Similar behaviour was observed for all the studied $ReBaCo_{2-x}Mn_xO_{5+\delta}$, also regarding the overall equilibrium values at high temperatures. Choice of Re^{3+} has also profound effect on the oxygen content, with higher values observed for larger rare earth cations. Unfortunately, substitution of cobalt with manganese causes rather considerable deterioration of the transport characteristics of $ReBaCo_{2-x}Mn_xO_{5+\delta}$. The cause of such behaviour, as explained above, is associated with change of concentration of the charge carriers, but also with change of the oxygen content in the compounds at high temperatures. Nevertheless, for materials with moderate Mn content, maximal values of total electrical conductivity still is high and exceeds 100 S cm^{-1} (i.e. 220 S cm^{-1} at 400 °C for $PrBaCo_{1.5}Mn_{0.5}O_{5+\delta}$ [35], 200 S cm^{-1} at 400 °C for $NdBaCo_{1.5}Mn_{0.5}O_{5+\delta}$ [39], 200 S cm^{-1} at 700 °C for $GdBaCo_{1.4}Mn_{0.6}O_{5+\delta}$ [18]). Further increase of manganese content leads to the decrease of maximum σ value to range from few to less than 50 S cm^{-1} when Mn content equal 1 or 1.5 (i.e. 45 S cm^{-1} at 700 °C for $PrBaCoMnO_{5+\delta}$ [this work], 20 S cm^{-1} at 700 °C for $NdBaCoMnO_{5+\delta}$ [this work], 25 S cm^{-1} at 1200 °C for $GdBaCoMnO_{5+\delta}$ [18], 20 S cm^{-1} at 1200 °C for $GdBaCo_{0.8}Mn_{1.2}O_{5+\delta}$ [18]).

From the application point of view, cathodic polarization resistance (R_p) is one of the most important parameters describing the manufactured cathode. It is widely accepted that at a given temperature effective operation of the cathode requires that R_p value does not exceed 0.15 Ω cm^2 [51]. In Tab. 2, cathodic polarization resistances are gathered, which were registered at different temperatures for selected $ReBaCo_{2-x}Mn_xO_{5+\delta}$-based cathodes (pure compound or composite-type) prepared with screen-printing method. Moreover, exemplary EIS data recorded with electrochemical spectroscopy impedance technique in 800-900 °C temperature range (Fig. 5a) for composite $NdBaCoMnO_{5+\delta}$-LSGM (60:40 wt. %) cathode, as well as its relation between polarization resistance and temperature in Arrhenius plot (Fig. 5b), are presented.

Tab. 2 Cathodic polarization resistance (R_p) recorded for $ReBaCo_{2-x}Mn_xO_{5+\delta}$-based cathodes. Measurements conducted on electrolyte-supported symmetric cells.

Chemical composition of the cathode	R_p [Ω cm^2]	Temperature [°C]	Ref.
$GdBaCo_2O_{5+\delta}$	0.070	700	[5]
$GdBaCo_{1.5}Mn_{0.5}O_{5+\delta}$	0.040 / 0.551	850 / 700	this work
$NdBaCo_{1.5}Mn_{0.5}O_{5+\delta}$	0.070 / 0.384	850 / 700	[35]
$NdBaCoMnO_{5+\delta}$-LSGM composite (60:40 wt. %)	0.083 / 0.171	850 / 800	this work
$GdBaCo_{1.8}Mn_{0.2}O_{5+\delta}$-CGO composite (70:30 wt. %)	0.075	650	[18]
$GdBaCo_{1.4}Mn_{0.6}O_{5+\delta}$-CGO composite (70:30 wt. %)	0.082	650	[18]

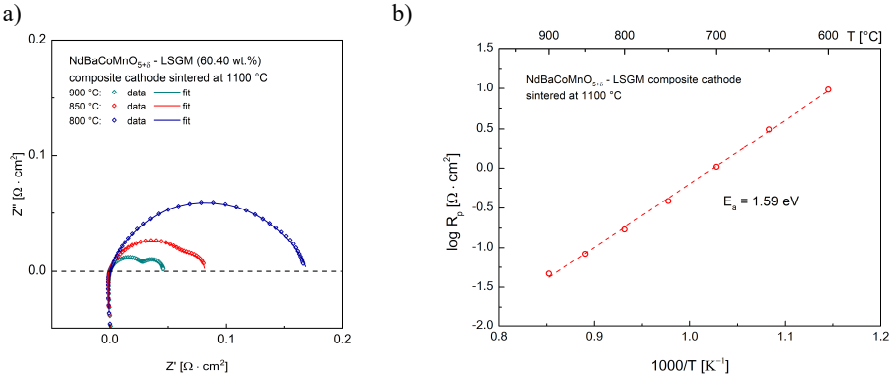

Fig. 5 a) EIS data of the polarization resistance and **b)** polarization resistance as a function of temperature for the symmetric cell with composite $NdBaCoMnO_{5+\delta}$-LSGM (60:40 wt. %) cathode.

Mn substitution into parent $ReBaCo_2O_{5+\delta}$ causes an increase of the cathodic polarization resistance, however, with significantly reduced value of TEC such doping may be still beneficial. As shown in Tab. 1, two strategies of cathode designing are favourable, introduction of bigger Re^{3+} or preparation of composite electrodes (sintered mixture of cathode and electrolyte powders). In the first case, i.e. for moderate Mn content (0.5 mol) complete substitution of smaller Gd^{3+} with bigger Nd^{3+} leads to significant decrease of R_p and consequently such cathode can effectively work in the vicinity of 800 °C [35]. Simultaneously, preparation of a composite cathodes leads to further, significant decrease of the polarization resistance and in such a case even small Re^{3+} (i.e. Gd^{3+}) can be applied. Proper selection of both cathode's and electrolyte's chemical composition, as well as optimization of theirs weight ratio may lead to obtaining electrodes working effectively even at temperature as low as 650 °C. Further decreasing of the working temperature is considered as possible, but only if anode-supported construction with a thin layer of the electrolyte is implemented, while at the same time, microstructure of the cathode material is also significantly modified e.g. through usage of nanoscale materials (such as nanofibers). In this aspect, one of the leading methods is electrospinning, which allows to obtain electrode layers with interconnected needle-like microstructure, greatly enhancing catalytic activity at lower temperatures [52-54].

7 Summary

Nowadays, development of Solid Oxide Fuel Cells is focused on decreasing of their working temperature, which is expected to significantly extend their lifetime, increase the

efficiency and decrease costs of the main components. Progress in achieving of this goal is hindered mostly by poor catalytic activity of the cathode materials. In this work, we discussed an overview of $ReBaCo_{2-x}Mn_xO_{5+\delta}$-based candidate cathode materials regarding their application at lowered temperatures. It is shown that proper doping strategy (amount of Mn, choice of Re^{3+}) may positively impact thermomechanical properties, and while some deterioration of the transport properties occurs, it is possible to prepare pure or composite-type $ReBaCo_{2-x}Mn_xO_{5+\delta}$-based cathode layers exhibiting relatively low polarization resistance. The so far presented efforts allowed to design and manufacture effectively working $ReBaCo_{2-x}Mn_xO_{5+\delta}$ cathode materials at high and intermediate temperatures. However, it seems that designing of the cathode, which can exhibit desired level of activity at lower temperatures, must be accompanied also by suitable microstructural modifications.

Acknowledgements: The project was funded by the Polish Ministry of Science and Higher Education (MNiSW) on the basis of the decision number 0128/DIA/2016/45.

References

1. A. Grimaud, K.J. May, C.E. Carlton, Y.-L. Lee, M. Risch, W.T. Hong, J. Zhou, Y. Shao-Horn, Nat. Commun. **4**, 1–7 (2013)
2. H. Fan, M. Keane, P. Singh, M. Han, J. Power Sources. **268**, 634–639 (2014)
3. L. Zhao, J. Shen, B. He, F. Chen, C. Xia, Int. J. Hydrogen Energy. **36**, 3658–3665 (2011)
4. M.A. Peña, J.L.G. Fierro, Chem. Rev. **101**, 1981–2017 (2001)
5. R. Pelosato, G. Cordaro, D. Stucchi, et. al. J. Power Sources. **298**, 46–67 (2015)
6. J.H. Kim, A. Manthiram, J. Mater. Chem. A. **3**, 24195–24210 (2015)
7. N. Mahato, A. Banerjee, A. Gupta et. al. Prog. Mater. Sci. **72**, 141–337 (2015)
8. Z. Du, H. Zhao, C. Yang, Y. Shen et. al. , J. Power Sources. **274**, 568–574 (2015)
9. S. Liu, W. Zhang, Y. Li, B. Yu, RSC Adv. **7**, 16332–16340 (2017)
10. C. Fu, K. Sun, N. Zhang, X. Chen, D. Zhou, Electrochim. Acta. **52**, 4589–4594 (2007)
11. J.-H. Kim, A. Manthiram, J. Electrochem. Soc. **155**, B385 (2008)
12. E. Wachsman, T. Ishihara, J. Kilner, Low-temperature solid-oxide fuel cells, MRS Bull. **39**, 773–779 (2014) doi:10.1557/mrs.2014.192.
13. D.S. Tsvetkov, I.L. Ivanov, A.Y. Zuev, J. Solid State Chem. **199**, 154–159 (2013)
14. M. Han, X. Tang, H. Yin, S. Peng, J. Power Sources. **165**, 757–763 (2007)
15. C. Lim, A. Jun, H. Jo, K.M. Ok, J. Shin et. al. , J. Mater. Chem. A. **4**, 6479–6486 (2016)
16. D.S. Tsvetkov, I.L. Ivanov, I. V et. al. , Thermochim. Acta. **519**, 12–15 (2011)
17. A.C. Tomkiewicz, M. Meloni, S. McIntosh, Solid State Ionics. **260**, 55–59 (2014)
18. D. Muñoz-Gil, E. Urones-Garrote, D. Pérez-Coll, U. Amador, S. García-Martín, J. Mater. Chem. A. **6**, 5452-5460 (2018)
19. W. He, F.-F. Dong, X.-L. Wu, M. Ni, *Adv. Sustain. Syst.* **1**, 1700005 (2017)
20. J. Hou, L. Bi, J. Qian, Z. Gong, Z. Zhu, W. Liu, J. Power Sources. **301**, 306–311 (2016)
21. M. Li, W. Zhou, V.K. Peterson, M. Zhao, Z. Zhu, J. Mater. Chem. A. **3**, 24064–24070 (2015)
22. M. Li, M. Zhao, F. Li, W. Zhou, V.K. Peterson, X. Xu, Z. Shao, I. Gentle, Z. Zhu, Nat. Commun. **8**, 1–9 (2017)
23. S. Zhuiykov, *Nanostructured Semiconductors*, (Woodhead Publishing, 2018), ISBN: 978-0-08-101920-7
24. Z. Gao, L. V. Mogni, E.C. Miller, J.G. Railsback, S.A. Barnett, Energy Environ. Sci. **9**, 1602–1644 (2016)
25. B. O. Omondi, E.C.S. Transactions **68**, 903–917 (2015)
26. W. Zhan, Y. Zhou, T. Chen, G. Miao, X. Ye, J. Li, Z. Zhan, S. Wang, Z. Deng, Int. J. Hydrogen Energy. **40**, 16532–16539 (2015)

27. J. Hwang, R.R. Rao, L. Giordano, Y. Katayama, Y. Yu, Y. Shao-Horn, Science **358**, 751–756 (2017)
28. Y. Chen, Y. Lin, Y. Zhang, S. Wang, D. Su, Z. Yang, M. Han, F. Chen, Nano Energy. **8**, 25–33 (2014)
29. G. Centi, S. Perathoner, Microporous Mesoporous Mater. **107**, 3–15 (2008)
30. M.A. Laguna-Bercero, J. Power Sources. **203**, 4–16 (2012)
31. J. Suntivich, H.A. Gasteiger, N. Yabuuchi, H. Nakanishi, J.B. Goodenough, Y. Shao-Horn, Nat. Chem. **3**, 546–550 (2011)
32. B.P. Uberuaga, G. Pilania, Chem. Mater. **27**, 5020–5026 (2015)
33. G. King, P.M. Woodward, J. Mater. Chem. **20**, 5785–5796 (2010)
34. J.B. Goodenough, J. Phys. Chem. Solids. **6**, 287–297 (1958)
35. A. Olszewska, Z. Du, K. Świerczek, H. Zhao, B. Dabrowski, J. Mater. Chem. A. **6**, 13271-13285 (2018)
36. J.-H. Kim, L. Mogni, F. Prado, A. Caneiro, J.A. Alonso, A. Manthiram, J. Electrochem. Soc. **156**, B1376 (2009)
37. A.S. Urusova, V.A. Cherepanov, O.I. Lebedev, T. V Aksenova, L.Y. Gavrilova, V. Caignaert, B. Raveau, J. Mater. Chem. A. **2**, 8823–8832 (2014)
38. G. Kostogloudis, Solid State Ionics. **118**, 241–249 (1999)
39. T. Broux, M. Bahout, J.M. Hanlon, O. Hernandez, S. Paofai, A. Berenov, S.J. Skinner, J. Mater. Chem. A. **2**, 17015–17023 (2014)
40. X. Huang, J. Feng, H.R.S. Abdellatif, J. Zou, G. Zhang, C. Ni, Int. J. Hydrogen Energy. **43**, 8962–8971 (2018)
41. K. Świerczek, N. Yoshikura, K. Zheng, A. Klimkowicz, Solid State Ionics. **262**, 645–649 (2014)
42. H.Y. Lee, K. Huang, J.B. Goodenough, J. Electrochem. Soc. **145**, 3220–3227 (1998)
43. S.O. Choi, M. Penninger, C.H. Kim, W.F. Schneider, L.T. Thompson, ACS Catal. **3**, 2719–2728 (2013) doi:10.1021/cs400522r.
44. D. Chen, R. Ran, K. Zhang, J. Wang, Z. Shao, J. Power Sources. **188** (2009) 96–105
45. X. Kong, H. Sun, Z. Yi, B. Wang, G. Zhang, G. Liu, Ceram. Int. **43**, 13394–13400 (2017)
46. W. Guo, R. Guo, L. Liu, G. Cai, C. Zhang, C. Wu, Z. Liu, H. Jiang, Int. J. Hydrogen Energy. **40**, 12457–12465 (2015)
47. P.G. Radaelli, S.W. Cheong, Phys. Rev. B - Condens. Matter Mater. Phys. **66**, 1–9 (2002)
48. S. Zhou, X. Miao, X. Zhao, C. Ma, Y. Qiu, Z. Hu, J. Zhao, L. Shi, J. Zeng, Nat. Commun. **7**, 1–7 (2016)
49. C. Zobel, M. Kriener, D. Bruns, J. Baier, M. Grüninger, T. Lorenz, P. Reutler, A. Revcolevschi, Phys. Rev. B - Condens. Matter Mater. Phys. **66**, 1–4 (2002)
50. A. Olszewska, K. Świerczek, W. Skubida, Z. Du, H. Zhao, B. Dabrowski, J. Phys Chem., **123**, 46-61 (2019)
51. R. Pelosato, A. Donazzi, G. Dotelli, C. Cristiani, I. Natali Sora, M. Mariani, J. Eur. Ceram. Soc. **34**, 4257–4272 (2014)
52. L. Fan, B. Zhu, P.C. Su, C. He, Nano Energy. **45**, 148–176 (2018)
53. X. Wang, M. Afzal, H. Deng, W. Dong, B. Wang, Y. Mi, Z. Xu, W. Zhang, C. Feng, Z. Wang, Y. Wu, B. Zhu, Int. J. Hydrogen Energy. **42**, 17552–17558 (2017)
54. Y. Chen, Y. Bu, Y. Zhang, R. Yan, D. Ding, B. Zhao, S. Yoo, D. Dang, R. Hu, C. Yang, M. Liu, Adv. Energy Mater. **7**, 1–7 (2017)